López et al., J Nanomater Mol Nanotechnol 2013, 2:4
http://dx.doi.org/10.4172/2324-8777.1000117

Journal of Nanomaterials & Molecular Nanotechnology

Research Article

A SCITECHNOL JOURNAL

Occlusion of INTERFERON® and COPAXONE® on SBA-15 Silica Reservoirs for their Use in the Treatment of Demyelization Diseases

Tessy López[1,2,3], Emma Ortiz-Islas[2*], Miriam López[2], José Flores[4] and Teresa Corona[4]

Abstract

Interferon® and Copaxone®, two commercial drugs used to treat the demyelization diseases like multiple sclerosis, were adsorbed on nanostructured SBA-15 reservoir. SBA-15 is ordered mesoporous silica normally used as catalytic adsorbent powder, but in this work we occluded the drug in the solid from separate solutions of each drug and then released them in a controlled way. The resultant SBA15-Copaxone and SBA15-Interferone were characterized by means of Infrared spectroscopy, Electron Microscopy, N_2 adsorption-desorption, Thermal-gravimetric analysis and X-ray diffraction techniques. Also, an "*in vitro*" drug release test was performed using an aqueous medium, the released drug was monitored by Ultraviolet-Visible spectroscopy. The resultant X-ray diffraction patterns and electron micrographs showed the characteristic ordered structures of mesoporous silica nanomaterials. The calculated surface area, pore diameter and pore volume values for the silica containing the drugs decreased approximately a 50% compared to SBA-15 reference values. These observations suggest that the drug molecules occupied the empty spaces inside and on the surface of the samples. The drug release profiles showed two stages, beginning with fast medicament liberation during the first hours, followed by a slow drug release until the end of the test.

Keywords

SBA-15; Drug release; Demyelization disease; Interferon; Copaxone

Introduction

Silica is a widely used material in adsorption, separation, catalysis and sensors applications. However, it has several important uses in biological and biotechnological fields due to its well demonstrated biocompatible properties. Currently, interest on silica as a drug vehicle and controlled release device has increased. There are three main kinds of silica-based materials used as drug carriers: 1) Silica xerogels [1-4], 2) Mesoporous ordered silica (MCM-41 and SBA-15) [5-7] and 3) Mesoporous hollow silica spheres [8,9]. These ordered mesoporous silica have several attractive features for their potential application as drug release carriers: large surface areas, malleable pore sizes, controllable particle sizes and shapes, and easy surface's dual-functionalization (exterior and interior) [10]. SBA-15 is constituted of an array of hexagonally ordered channels and large internal volumes. Drugs can be adsorbed through a diffusion process, and can be released over different periods of time depending on the drug characteristics (size and chemical composition), release medium, pore size, particle size and morphology. Drug release can occur over minutes, hours or days [11-13] into simulated body fluid, phosphate buffered saline [14-18] or in a specific tissue of the body. SBA-15 has been able to store therapeutically relevant drugs ranging from neurological drugs [19,20], antibiotics [12,13], chemotherapeutic [21] and others [1,22].

Biocompatibility is one of the most important requirements for any material to be used in medical applications. In this sense, amorphous silica is considered nontoxic, biocompatible and degradable in living tissue [13,23,24]. We used SBA-15 as carries of cortisol, phenytoin and collagen-polyvinylpyrrolidone and released them in animal models. We found that drug was released in a prolonged time and that SBA-15 was highly biocompatible with the brain tissue and body's tissue of Wistar rats [25].

These two important features of SBA-15 (morphology and biocompatibility) allowed us to use SBA-15 silica material as carrier for immunomodulatory agents COPAXONE (CPX) and INTERFERONE (INT), which are used for the treatment of Multiple Sclerosis (MS) [26]. MS is a chronic, potentially highly disabling disorder with considerable social impact and economic consequences. Four immunomodulatory treatments (glatiramer acetate and three interferon-b preparations) and two immunosuppressant (natalizumab and mitoxantrone) are now approved for the treatment of MS and allow the frequency of attacks to be diminished and the progression of disability to be slowed, at least in the shorten medium-term. In addition, a number of new strategies have been developed for the treatment of the disease, such as novel immunomodulators (including antibodies/immunosuppressants), therapeutic strategies targeting leukocyte differentiation molecules, costimulatory molecules, anti-adhesion molecules, chemotaxis, autologous stem cell transplantation, anti-infectious therapies and strategies for neuroprotection, neurorepair and remyelination [27-29].

The aim of this work is the administration of immunomodulatory agents to MS in a controlled way during prolonged times maintaining their therapeutic effects, in order to reduce side effects caused by the drug when administered by systemic via.

Materials and Methods

Sample preparation

SBA-15: The sample was prepared according to Zhao et al. [30], following the next procedure: Four grams of Pluronics P123 block copolymer (BASF, Florham Park, New Jersey) were dissolved in an aqueous solution of 2 M HCl. The temperature of the solution was raised to 35°C, and TEOS (Aldrich, St. Louis, Missouri) was added dropwise to the system while vigorously stirring for 5 minutes. The stirring rate was then lowered and kept at this rate for 20 hours.

***Corresponding author:** Emma Ortiz-Islas, Nanotechnology Laboratory, National Institute of Neurology and Neurosurgery "MVS", Avenida Insurgentes Sur 3877, La Fama, Tlalpan, 14269, México D. F., México, Tel: (52) 55 56063822; ext 5034; E-mail: emma170@hotmail.com

Received: June 19, 2013 **Accepted:** July 29, 2013 **Published:** August 06, 2013

doi:http://dx.doi.org/10.4172/2324-8777.1000117

Subsequently the reacting mixture was heated to 80°C during 24 hours. The resulting white precipitate was separated from the liquid phase by filtering and further washed with deionized water. Finally, the polymer was removed by calcination in air at 550°C for 6 hours. The nominal molar composition for this synthesis was: 0.041 TEOS:6.67 H_2O:0.24 HCl:0.0007 P123.

SBA-15 impregnation: 1 g of SBA-15 powder was added to 20 ml of a saline solution containing 2 mg of Copaxone® (TEVA Pharmaceutical Industries LTD, Kfar Saba, Israel). Afterwards, the mixture was stirred during 24 hours and then water was removed by evaporation. The SBA-15-CPX sample was dried at 40°C for 3 days. The same procedure described above was used to impregnate SBA-15 with Interferone® (Biogen Idec Limited, Berkshire, United Kingdom). In this case we used a saline solution containing 3 µg of INT.

Characterization

Nitrogen adsorption-desorption: Adsorption-desorption nitrogen isotherms were obtained from a Micrometrics ASAP 2020 apparatus (BEL Japan Inc, Osaka, Japan) at the temperature of liquid nitrogen. The surface area was determined applying the BET equation, while the pore size and the pore volume were determined through BJH method using the desorption isotherm. Previous to nitrogen measures, the samples were treated with vacuum during 24 hours and only the SBA-15 sample was heated at 200°C, while the samples containing the drugs were heated at 30°C.

X-ray powder diffraction (XRD): Each sample was packed in a glass holder to be measured in a Bruker Advanced D-8 diffractometer which uses CuKα radiation ((Bruker Corp, Billerica, MA, USA). The diffraction patterns were obtained at room temperature. Diffraction intensities were measured at small angles between 0.6° to 4.0° with a step of 0.02° for 10 s per point.

Transmission Electron Microscopy (TEM): The Transmission Electron Microscopy (TEM) was used to determine the morphology of the samples using an LEO EM910 Carl Zeiss microscope with acceleration of 120 KV (Carl Ziess, Oberkochen, Germany).

Scanning Electron Microscopy (SEM): For the SEM studies a JEOL 5600 LV equipped with an EDS (Carl Ziess, Oberkochen, Germany) attachment for chemical analysis was used to perform the morphological composition of the samples.

Fourier Transformed Infra Red Spectroscopy (FTIR): In this study we used the KBr method; mixing each SBA-15-drug material with KBr in a ratio of 5 wt%. Each mixture was pressed into a translucent wafer and measured in an IR-Affinity-1 Shimadzu Spectrophotometer (SHIMADZU CORPORATION, Tokyo, Japan). The spectra were recorded in the medium infrared from 4000 to 400 cm^{-1}.

Thermal Gravimetric Analysis (TGA): Weight loss % in each sample was determined by thermogravimetry using a SAT-*i* 1000 equipment (Instrument Specialists Inc., Wisconsin, USA). The samples were heated from room temperature up to 800°C at a speed of 10°C/min under a nitrogen flux.

Drug release tests

Each SBA-15-drug powder was pressed into to a tablet of 50 mg approximately and immersed in 200 ml of deionized water. At determined times one aliquot of 4 ml was removed for its measurement by UV spectroscopy in an S-3100 SCINCO spectrophotometer (SCINCO CO., LTD, Seoul, Korea). After the measurement, the aliquot was returned to the original solution. A calibration curve with known concentration of the drug versus absorbance's intensity was used to quantify the released drug. The increment of the absorbance was monitored at 190 nm. The concentration of the released drug in each time was determined by the interpolation of each absorbance obtained in the calibration curve.

Results and Discussion

The low angle XRD pattern of SBA-15 is shown in Figure 1. The figure shows a sharp peak at 2θ=0.98 and two small peaks at 2θ=1.6 and 1.94. These signals are indexed as (100), (110) and (200) reflections of p6mm symmetry, indicating ordered hexagonal arrays [23,30]. The Bragg's law was applied to reflection (100) finding that the distance between the centers of adjacent cylinders was104 Å.

TEM images of SBA-15 and SBA 15-CPX and SBA 15-INT are displayed in Figure 2. The Figure 2a shows the formation of cylindrical channel arrays on pure SBA-15. While, the Figure 2c shows that the cylinder's open-ends have a hexagonal shape. The cylinders have approximately an average diameter of 10 nm with a wall thickness

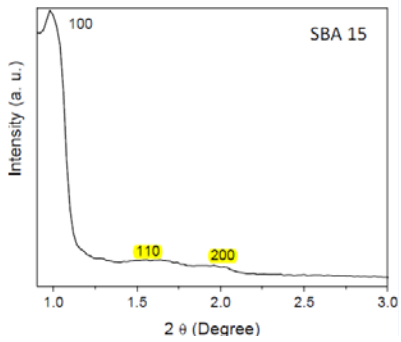

Figure 1: X ray diffraction pattern at low diffraction angle of SBA-15.

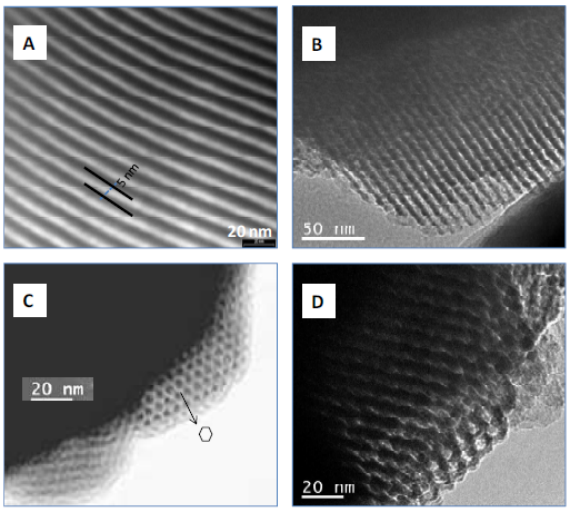

Figure 2: Transmission electron micrographics of pure SBA-15: (a) Cylindrical arrangement and (c) Ends of the cylinders with hexagonal shape. (b) TEM image of SBA 15-CPX. (d) TEM image of SBA 15-INT.

of around 5 nm (Figure 2a). Figure 2b and 2d correspond to SBA 15-CPX and SBA 15-INT samples respectively, which show the cylinders with hexagonal array of SBA 15 after it was impregnated with the commercial drugs. The TEM results are consistent with the low angle XRD result confirming the ordered meso-structure of SBA-15.

Nitrogen adsorption–desorption isotherms and pore distribution (insert) of SBA-15 and SBA-15 loaded with the drugs are presented in Figure 3. All materials derived N_2 adsorption-desorption type IV isotherms, which is a feature of mesoporous solids [31]. All isotherms contain a H1 hysteresis loop between P/P_0= 0.50–0.75, due to capillary condensation of nitrogen molecules into mesopores. The type H1 hysteresis loops observed in the mesopore range, indicate the existence of a two dimensional p6mm structure formed by the open-ended cylindrical mesopores. These samples have a narrow pore size distribution (Figure 3), which are characteristic of SBA-15 mesoporous matrixes. The textural values obtained from the N_2 isotherms are given in Table 1. There is a decrement in the values of the surface area (S_{BET}), and pore volume (V_p), after the drugs were loaded to SBA-15. Meanwhile, the pore size (D_p) increased slightly. The S_{BET} value for pure SBA-15 was 885 m^2/g and after drugs addition was 314 m^2/g. The V_p of the SBA-15 was 0.8172 cc/g and 0.54 cc/g for SBA-drugs.

The low values of S_{BET} and V_p of SBA15-CPX and SBA 15-INT samples, compared with pure SBA-15 have an explanation in the fact that drug molecules occupied these spaces when they were adsorbed in SBA-15. It is conceivable that the internal and external surface of the cylindrical pores were partially covered with the drug molecules. For this reason the isotherms found for these samples have the same shape that corresponding isotherm of pure SBA-15, but less nitrogen

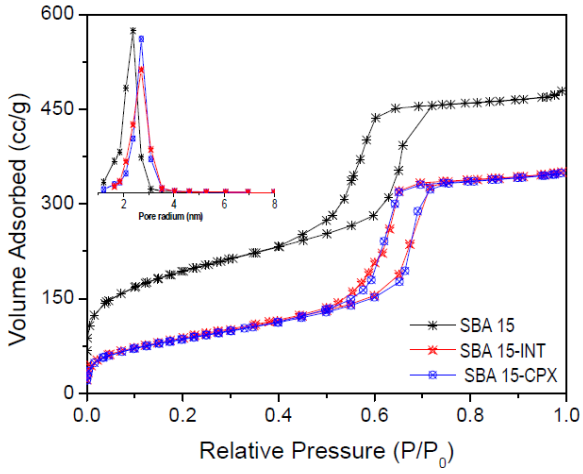

Figure 3: N_2 adsorption-desorption isotherms of pure SBA 15 and when it was impregnated with neurological drugs.

Table 1: Textural properties and Kinetics data obtained from Korsmeyer-Peppas equation fits of SBA-15 and SBA-15 containing INT and CPX drugs. S_{BET} is the surface area, D_p is the pore diameter, V_p is the pore volume, k is the kinetic constant, and n is the release exponent.

Sample	*SBET* (m^2/g)	D_p(nm)	V_p (cc/g)	*k*	*n*	r^2
SBA 15	885	4.3	0.8173			
SBA 15-CPX	314	5.0	0.542446	1.145 ± 0.001	0.075 ± 0.013	91
SBA 15-INT	315	4.9	0.539549	1.036 ± 0.003	0.219 ± 0.013	97

was needed to form their isotherms. We have observed the same behavior, when antiepileptic drugs were loaded on MCM-41 and SBA-15. We have schematically ascribed that drug molecules are packed inside the cylindrical channels without completely filling them, leaving some space where the nitrogen molecules were adsorbed later [19,32]. On the other hand, the insert in Figure 3 shows the pore size distribution. SBA-15 without any drug has a monomodal distribution with a maximum at 2.3 of pore radius and average pore size of 4.3 nm. When CPX drug was loaded on SBA-15 the average pore size was 5.0 nm. Finally, for the SBA15-INT sample the average pore diameter was 4.9 nm. The TEM and low angle XRD results are consistent with the N_2 adsorption-desorption observations confirming again that an ordered meso-structure of SBA-15 was obtained. However, last technique let us infer that SBA-15 structure was maintained unalterable even after the drugs were added into silica.

The sectioned FTIR spectra of pure SBA-15 and its impregnated forms are shown in Figure 4. The spectrum of SBA-15 (reference) shows the characteristic bands of an amorphous silica material. In Figure 4a, the band observed at 3450 cm^{-1} comes from stretching vibration modes of hydroxyl groups located on the silica's surface as silanol groups (≡Si-OH). This band and another small band observed at 1640 cm^{-1} in Figure 4b, which is associated to stretching δH-O-H symmetry vibrations in the water molecule, indicate that water is adsorbed on the silica's surface. The wide and intense band seen at 1080 cm^{-1} in Figure 4c with a shoulder at 1021 cm^{-1} are related with asymmetric stretching vibrations of siloxane groups (Si-O-Si). The band seen at 965 cm^{-1} is due to silanol bending vibrations, while, the others at 800 cm^{-1} and 460 cm^{-1}, are asymmetric bending Si–O–Si (νSiO) modes, and of bending vibrations Si–O–Si (δSi-O) modes, respectively (Figure 4d).

The spectra of SBA-15 with the drugs occluded seem to be similar as is shown in Figure 4a-4d. In both spectra it is possible to observe the characteristic bands, previously described, that identify silica. However, other several bands which are marked with arrows in Figure 4 appeared. In Figure 4a, a wide band that encloses signals of O-H, C-H and N-H stretching vibrations from the drugs is seen between 3900 cm^{-1} and 2820 cm^{-1}. In Figure 4b the signal at 1700 cm^{-1} is barely visible because it is overlapped with the band corresponding to water. This band can be assigned to νC=O stretching vibrations, from the drug too. In Figure 4b other two small signals related to C-H and N-H functional groups are observed at 1553 cm^{-1} and 1400 cm^{-1}. All these observations allow us to state that the all signals were generated from the drugs due to their structures are formed by amine-acid sequences (Figure 4b). Nevertheless, we need to make specific probes to identify very well these functional groups (elemental microanalysis and ^{13}C nuclear magnetic resonance). Also, in the spectra of silica-drug (Figure 4d) it is possible to view that the intensity of the band corresponding to silanol groups (≡Si-OH) decreased due to the interactions between surface silanol and functional groups (NH_2, COOH) of the drugs. It agrees with the observed in Figure 4a, where the bands correspond to Si-OH on samples containing the drug were shifted to less energies compared with the respective pure silica. We have attributed this phenomenon to the formation of weak bonds as hydrogen bridges or Van der Waals electrostatic interactions between the drug and the surface of the silica, stabilizing the drug within silica material [20].

The scanning micrographs of SBA-15 containing the drugs are shown in Figure 5. Both samples have the same structure, where the

doi:http://dx.doi.org/10.4172/2324-8777.1000117

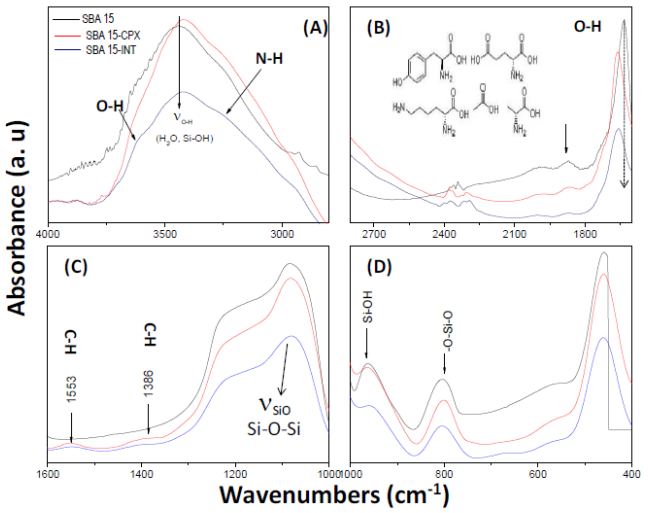

Figure 4: Sectioned FTIR spectra of SBA 15, SBA 15-CPX and SBA 15-ITN samples. (a) 4000-2800 cm^{-1}, (b) 2800-1600 cm^{-1} and CPX structure, (d) 1600-1000 cm^{-1}, and (d) 1000-400 cm^{-1}.

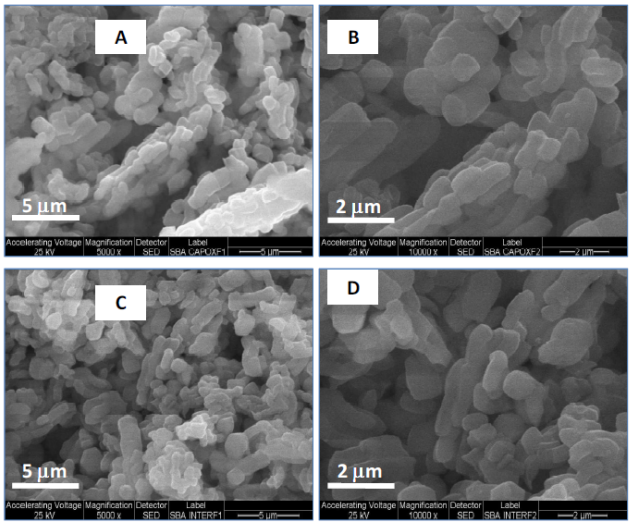

Figure 5: Scanning Electron Micrographs of SBA 15-CPX sample (A and B) and of SBA 15-ITN (C and D).

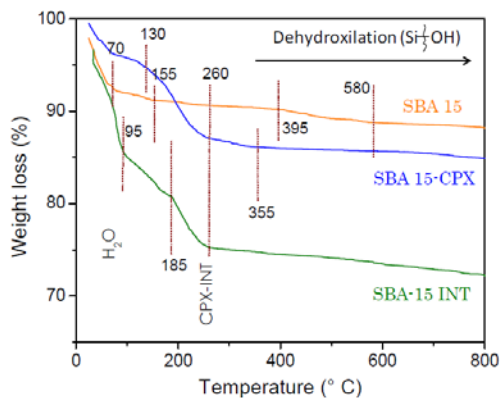

Figure 6: Thermo-graphs of SBA15, SBA15-CPX and SBA15-INT samples thermally treated.

typical worn-like forms are characteristic of SBA-15 are seen and have a size of 2-10 µm in length and 1-2 µm in diameter. SBA-15 unchanged its structure. The results have good agreement with the N_2 adsorption-desorption studies and suggest that the drug does not has any effect on the SBA15 structure.

In Figure 6 thermo-graphs of SBA-15, SBA15-CPX and SBA15-INT are displayed after being thermally treated. The graph corresponding to SBA-15 shows several weights loss. The first ones occurred at 70°C due to the removal of water adsorbed on silica's surface and residual solvent used during the synthesis. The second occurred at 155°C corresponding to total dehydration of the sample. One more was observed at 260°C induced by combustion of the residual organic material from the alkoxide used during the SBA-15 preparation. There are others two at 395 and 580°C occasioned by the surface dehydroxylation. SBA15-CPX thermo-graph shows also several weight losses. The first is seen at 70°C alike the sample before; it is due to dehydration of the sample and the solvent removal. There is a second weight loss at 130°C due to the dehydration of the samples. However, a remarkable change is observed at 350°C, which is attributed to the removal of organic matter from the drug, drug vehicle and organic precursors used on the silica synthesis. Other two small losses can be seen at 355 and at 580°C generated by the sustained dehydroxylation carried out in silica's surface. The thermal-profile of SBA15-INT has the same weight loss although in different percentage than the sample before. In SBA-15-INT the first loss was 9% carried out at 70°C and the second loss was 2.56% at 95°C. Both were due to sample dehydration and solvent removal. A third at 185°C had a higher weight loss (4.78%) due to dehydration, therefore, this observation only indicates that the sample was highly hydrated. At 260°C occurred other percentage of weight loss due to the removal organic substances like to drug, drug vehicle and organic precursors of the silica. After this point, two weight losses were observed at 395 and 580°C because as the other samples at these temperatures there is a surface dehydroxylation. The percentages of weight loss observed in each temperature are given in Table 2.

Figure 7 reports the calibration curve (Figure 7A) and the release profile of CPX carried out during 8 hours (Figure 7B). The curve shows a pronounced initial burst CPX release within the first 2 hours. After that time, a slow CPX release steps were seen. Figure 8 reports the calibration curve (Figure 8A) and the release profile of INT carried out during 8 hours (Figure 8B). From this curve is possible to deduce the two same drug release stages. However, after two hours the INT molecules are released faster than the CPX molecules. As we have previously stated, in the first stage the drug molecules adsorbed on the external surface of SBA15 and close to mouth of the channels are released quickly. In the second step the drug release is slow because the molecules have to leave from the channels. Also, in this second step the drug molecules into of the channel are interacting with the silanol groups, thus, it take more time to the molecules to get out

Table 2: Percentage of weight loss at different temperature of SBA-15 and its impregnated forms. Where %wl= percentage of weight loss.

°C/	70	95	130	155	185	260	355	395	580
Sample	**(%wl)**								
SBA 15	7.5			1.24		0.63		0.36	1.72
SBA15-CPX	3.67		1.54			7.6	0.72		0.73
SBA-INT	9	2.56			4.78	5.7		1.26	0.37

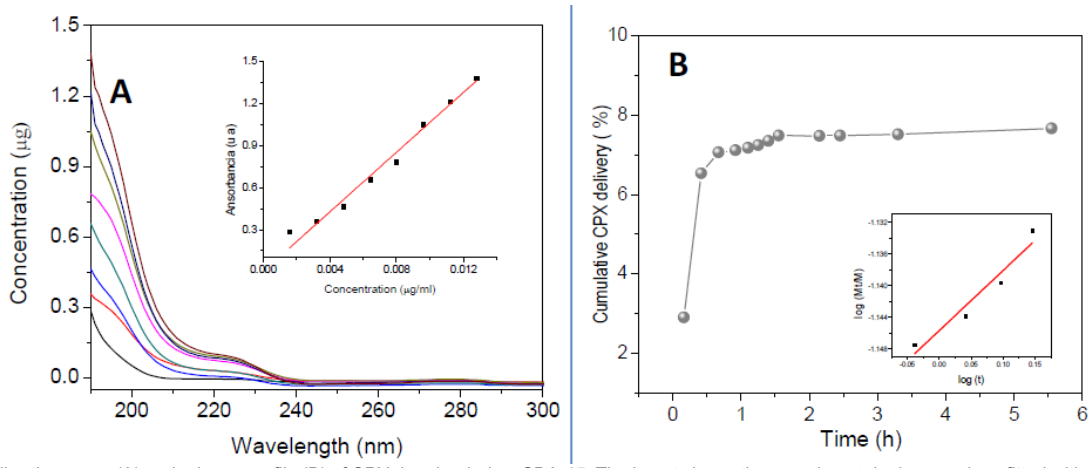

Figure 7: Calibration curve (A) and release profile (B) of CPX drug loaded on SBA-15. The insert shows the experimental release values fitted with the Korsmeyer-Peppas Peppas equation to obtain the "n" values.

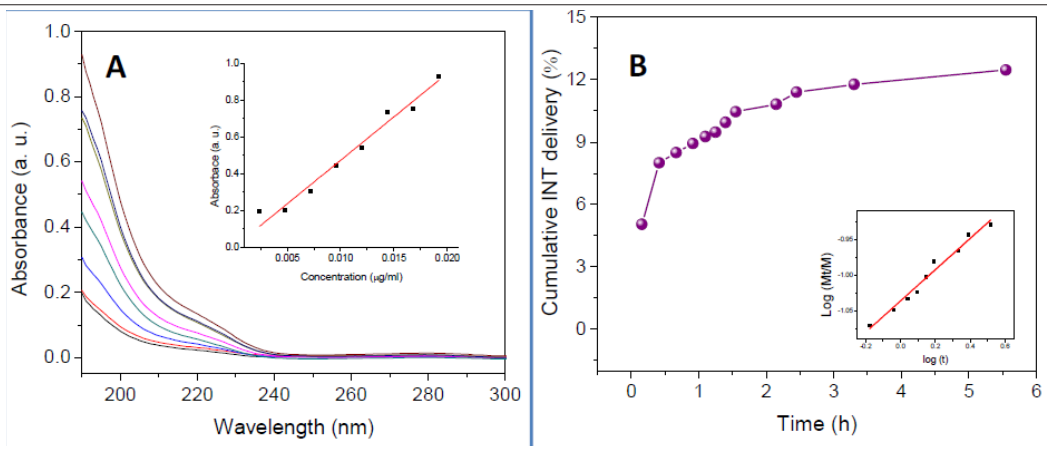

Figure 8: Calibration curve (A) and release profile (B) of INT drug loaded on SBA-15. The insert is showing the experimental release results fitted with the Korsmeyer-Peppas Peppas equation to obtain the "n" values.

from the silica channels [32].

There are several kinetic models that describe the mechanism of drug release from solid dosage forms. Drug release may follow mixed release mechanisms; it may involve both diffusion and dissolution controlled processes. Korsmeyer and Peppas developed an empirical equation to analyze both Fickian and non-Fickian release of drug from swelling as well as non-swelling polymeric delivery systems [33]. The equation is represented as:

$$Mt/M = Kt^n$$

The logarithm form of this equation could be written as:

$$\text{Log}\,(Mt/M) = \text{Log}\,k + n\,\text{Log}\,t$$

Where Mt/M is fraction of drug released at time t, n is diffusion exponent indicative of the mechanism of transport of drug through the polymer, k is kinetic constant incorporating structural and geometric characteristics of the delivery system. For Korsmeyer-Peppas model, the release exponent $n \leq 0.45$ is for Fickian diffusion release and $0.45<n<0.89$ for non-Fickian release; while $n=1$ is for zero order release. Although it mathematical model was developed to polymeric matrixes, for porous matrix structures, Peppas [34] has suggested that ***n*** assumes lower values.

To investigate the release mechanisms in the diffusion controlled stage, the in vitro drug release data were fitted with the Peppas' equation, in the period following the initial burst and before the quasi-steady state. The fitted graphics are shown in the inserts of the Figures 7B and 8B; while the fitted parameters are summarized in Table 1. The n values obtained for both samples are less than 0.5, indicative that the release mechanism is controlled by Fickian diffusion.

Conclusions

SBA-15 silica material was successfully used as reservoir of Interferone and Copaxone drugs and also as a releasing device in an aqueous medium. The morphology of SBA-15 and its impregnated forms with the drugs were well characterized. The impregnation with the drugs did not affect the structure of SBA-15. The drugs were released in two different ways: in the first stage, the kinetics was carried out by a solubility mechanism and in the second stage, the kinetics was governed by a diffusion mechanism.

References

1. Iafisco M, Margiotta N (2012) Silica xerogels and hydroxyapatite nanocrystals for the local delivery of platinum-bisphosphonate complexes in the treatment

of bone tumors: a mini-review. J Inorg Biochem 117: 237-247.

2. Maver U, Godec A, Bele M, Planinsek O, Gaberscek M, et al. (2007) Novel hybrid silica xerogels for stabilization and controlled release of drug. Int J Pharm 330: 164-174.
3. Munusamy P, Seleem M, Alqublan H, Tyler Jr. R, Sriranganathan N, et al. (2009) Targeted drug delivery using silica xerogel systems to treat diseases due to intracellular pathogens. Mat Sci Eng C: 2313-2318.
4. López T, Quintana P, Martínez JM, Esquivel D (2007) Stabilization of dopamine in nanosilica sol–gel matrix to be used as a controlled drug delivery system. J Non-Cryst Solids 353: 987-989.
5. Yang P, Gai S, Lin J (2012) Functionalized mesoporous silica materials for controlled drug delivery. Chem Soc Rev 41: 3679-3698.
6. Li Z, Barnes JC, Bosoy A, Stoddart JF, Zink JI (2012) Mesoporous silica nanoparticles in biomedical applications. Chem Soc Rev 41: 2590-2605.
7. Vallet-Regí M (2010) Nanostructured mesoporous silica matrices in nanomedicine. J Intern Med 267: 22-43.
8. Wang B, Meng W, Bi M, Ni Y, Cai Q, et al. (2013) Uniform magnesium silicate hollow spheres as high drug-loading nanocarriers for cancer therapy with low systemic toxicity. Dalton Trans 42: 8918-8925.
9. Wang T, Chai F, Fu Q, Zhang L, Liu H, et al. (2011) Uniform hollow mesoporous silica nanocages for drug delivery in vitro and in vivo for liver cancer therapy. J Mater Chem 21: 5299-5306.
10. Kobler J, Möller K, Bein T (2008) Colloidal suspensions of functionalized mesoporous silica nanoparticles. ACS Nano 2: 791-799.
11. Areva S, Aäritalo V, Tuusa S, Jokinen M, Lindén M, et al. (2007) Sol-Gel-derived TiO2-SiO2 implant coatings for direct tissue attachment. Part II: Evaluation of cell response. J Mater Sci Mater Med 18: 1633-1642.
12. Meseguer-Olmo L, Ros-Nicolás M, Vicente-Ortega V, Alcaraz-Baños M, Clavel-Sainz M, et al. (2006) A bioactive sol-gel glass implant for in vivo gentamicin release. Experimental model in Rabbit. J Orthop Res 24: 454-460.
13. Radin S, El-Bassyouni G, Vresilovic EJ, Schepers E, Ducheyne P (2005) In vivo tissue response to resorbable silica xerogels as controlled-release materials. Biomaterials 26: 1043-1052.
14. Izquierdo-Barba I, Colilla M, Manzano M, Vallet-Regí M (2010) In vitro stability of SBA-15 under physiological conditions. Micropor Mesopor Mat 132: 442-452.
15. Pasqua L, Testa F, Aiello R, Cundari S, Nagy JB (2007) Preparation of bifunctional hybrid mesoporous silica potentially useful for drug targeting. Micropor Mesopor Mat 103: 166-173.
16. Clifford NW, Iyer KS, Raston CL (2008) Encapsulation and controlled release of nutraceuticals using mesoporous silica capsules. J Mater Chem 18: 162-165.
17. Carino IS, Pasqua L, Testa F, Aiello R, Puoci F, et al. (2007) Silica-based mesoporous materials as drug delivery system for methotrexate release. Drug Deliv 14: 491-495.
18. Ruiz-Hernandez E, Lopez-Noriega A, Arcos D, Izquierdo-Barba I, Terasaki O, et al. (2007) Aerosol-assisted synthesis of magnetic mesoporous silica spheres for drug targeting. Chem Mater 19: 3455-3463.
19. López T, Basaldella EI, Ojeda ML, Manjarrez J, Alexander-Katz R (2006) Encapsulation of valproic acid and sodic phenytoine in ordered mesoporous SiO_2 solids for the treatment of temporal lobe epilepsy. Opt Mater 29: 75-81.
20. López T, Bata-García JL, Esquivel D, Ortiz-Islas E, Gonzalez R, et al. (2010) Treatment of Parkinson's disease: nanostructured sol-gel silica-dopamine reservoirs for controlled drug release in the central nervous system. Int J Nanomedicine 6: 19-31.
21. Lu J, Liong M, Li Z, Zink JI, Tamanoi F (2010) Biocompatibility, biodistribution, and drug-delivery efficiency of mesoporous silica nanoparticles for cancer therapy in animals. Small 6: 1794-1805.
22. Seleem MN, Munusamy P, Ranjan A, Alqublan H, Pickrell G, et al. (2009) Silica-antibiotic hybrid nanoparticles for targeting intracellular pathogens. Antimicrob Agents Chemother 53: 4270-4274.
23. Lopez T, Ortiz E, Alexander-Katz R, Basaldella E, Bokhimi X (2009) Cortisol controlled release by mesoporous silica. Nanomedicine 5: 170-177.
24. Chia S, Urano J, Tamanoi F, Dunn B, Zink JI (2000) Patterned Hexagonal Arrays of Living Cells in Sol-Gel Silica Films. J Am Chem Soc 122: 6488-6489.
25. López T, Krötzsch E, Ortiz-Islas E, Alvarez-Lemus M, Balsadella E (2009) Release properties and acute biosecurity determination of collagen-polyvinylpyrrolidone loaded in ordered mesoporous silica. Key Eng Materials 391: 169-184.
26. Murray TJ (2006) Diagnosis and treatment of multiple sclerosis. BMJ 332: 525-527.
27. Murray TJ (2009) The history of multiple sclerosis: the changing frame of the disease over the centuries. J Neurol Sci 277: S3-S8.
28. Maier LM, Lowe CE, Cooper J, Downes K, Anderson DE, et al. (2009) IL2RA genetic heterogeneity in multiple sclerosis and type 1 diabetes susceptibility and soluble interleukin-2 receptor production. PLoS Genet 5: e1000322.
29. Oksenberg JR, Barcellos LF (2000) The complex genetic aetiology of multiple sclerosis. J Neurovirol 6: S10-S14.
30. Zhao D, Feng J, Huo Q, Melosh N, Fredrickson GH, et al. (1998) Triblock copolymer syntheses of mesoporous silica with periodic 50 to 300 angstrom pores. Science 279: 548-552.
31. Gregg SJ, Sing KSW (1982) Surface Area and Porosity. Adsorption. (2nd edn), Academic Press, New York, USA.
32. Lopez T, Ortiz E, Meza D, Basaldella E, Bokhimi X, et al. (2011) Controlled release of phenytoin for epilepsy treatment from titania and silica based materials. Mater Chem Phys 126: 922–929.
33. Korsmeyer RW, Peppas NA (1984) Solute and penetrant diffusion in swellable polymers. III. Drug release from glassy poly(HEMA-co-NVP) copolymers. J Control Rel 1: 89-98.
34. Peppas NA (1985) Analysis of Fickian and non-Fickian drug release from polymers. Pharm Acta Helv 60: 110-111.

Author Affiliations

Top

[1]*Nanotechnology and Nanomedicine Laboratory. UAM-Xochimilco. Calzada del Hueso 1100, Col. Villa Quietud, Coyoacán, 04960, México, D. F., México.*
[2]*Nanotechnology Laboratory. National Institute of Neurology and Neurosurgery "MVS". Avenida Insurgentes Sur 3877, La Fama, Tlalpan, 14269, México D. F., México*
[3]*Departament of Chemical and Molecular Engineering. Tulane University, New Orleans, USA.*
[4]*Neurodegenerative Disease Clinical Laboratory, National Institute of Neurology and Neurosurgery "MVS", Avenida Insurgentes Sur 3877, La Fama, Tlalpan, 14269, México D. F. México.*